

Spatial Constraint Generation for Motion Planning in Dynamic Environments

Han Hu^{1*} and Peyman Yadmellat²

Abstract—This paper presents a novel method to generate spatial constraints for motion planning in dynamic environments. Motion planning methods for autonomous driving and mobile robots typically need to rely on the spatial constraints imposed by a map-based global planner to generate a collision-free trajectory. These methods may fail without an offline map or where the map is invalid due to dynamic changes in the environment such as road obstruction, construction, and traffic congestion. To address this problem, triangulation-based methods can be used to obtain a spatial constraint. However, the existing methods fall short when dealing with dynamic environments and may lead the motion planner to an unrecoverable state. In this paper, we propose a new method to generate a sequence of channels across different triangulation mesh topologies to serve as the spatial constraints. This can be applied to motion planning of autonomous vehicles or robots in cluttered, unstructured environments. The proposed method is evaluated and compared with other triangulation-based methods in synthetic and complex scenarios collected from a real-world autonomous driving dataset. We have shown that the proposed method results in a more stable, long-term plan with a higher task completion rate, faster arrival time, a higher rate of successful plans, and fewer collisions compared to existing methods.

I. INTRODUCTION

Motion planning in a dynamic environment is a cornerstone of autonomous driving and a challenging engineering problem. Motion planning methods often require spatial constraints provided by semantic maps (*e.g.*, centerline, lane boundary) to generate a trajectory. This requirement results in motion planning failure where the spatial constraint is absent or invalid; unmapped roads, unstructured open areas, congested traffic, partially obstructed single lane, etc.

To address this issue, we propose a new method to generate spatial constraints from the triangulation mesh of an environment that can be applied to autonomous driving. Existing triangulation-based path planning methods construct a triangulation mesh from nodes in the environment. The nodes can be the vertices of objects or center of objects. Subsequently, a channel which is a sequence of free triangles within the triangulation mesh, connecting the start location to the goal location, is found via a graph search method. The channel can serve as a spatial constraint for motion planning algorithms (*e.g.* Hybrid A* or Modified Funnel Algorithm). As the main advantage, the triangulation representation reduces the overall time complexity as it results

in a substantially smaller adjacency graph compared to grid-based methods [1].

Most known methods for motion planning inside a triangulation mesh (*e.g.* [1]–[7]) ignore dynamic objects, assume a static environment, and rely on repeated replanning to handle dynamic objects. These methods typically replan through dynamically maintained triangulation structure [8]–[11], incremental, or anytime variant search algorithms [12]–[14] for efficient replanning, or a combination of both. The primary challenge with these methods is that they are not flexible to changes in the environment. This is because the channel generation scheme in these methods often suffers from two fundamental limitations: a) invariant triangulation mesh connectivity assumption and b) masked dynamic nodes, which causes the channel. Combined, these two limitations can result in volatile and near-sighted path planning, which is not suitable for autonomous driving vehicles.

The first limitation is that the nodal connectivity of the triangulation mesh is assumed to be invariant over time. This is not a valid assumption as a subset of the channel no longer exist when the node connectivity changes. Motion planning based on a channel that does not exist can result in a near-sighted plan, leading to unfavorable situations such as path planner failures, sudden stops, and unrecoverable states. The second limitation is that the existing methods only consider the interaction between adjacent nodes. However, this approach causes the motion information of the non-adjacent dynamic nodes to be masked and ignored by the adjacent nodes' connectivity. As a result, the ego vehicle will have latent responses to dynamic nodes (*e.g.* pedestrians, vehicles).

To address the first limitation, we propose a novel, modular system to generate a sequence of connected channels segments. Each segment corresponds to a change in node connectivity at different points in time. This sequence of segments is generated by identifying the segment affected by the change and replacing it with a segment from the triangulation mesh connectivity after the change. We also propose a method to address the second limitation by transmitting distant nodes' motion information along the triangulation mesh edges. This is achieved by projecting each node's velocity vector to the adjacent nodes along the edges, thereby giving each node an estimated motion information of the distant nodes. Together, the proposed systems and method generate a sequence of channel segments. Each segment can be used by a motion planner as the spatial constraint to generate a partial trajectory, which is then combined into the overall plan, thereby finding a stable, long-term plan in

¹Department of Mechanical & Industrial Engineering, University of Toronto, Toronto, Ontario, Canada M5S 3G8

²Noah's Ark Lab., Huawei Technologies Canada, Markham, Ontario, Canada L3R 5A4

*The work was done during the author's internship at Noah's Ark Lab., Huawei Technologies Canada.

a dynamic environment.

The main contributions of this paper are:

- A spatial constraint generation system that predicts and plans in the triangulation mesh of the environment at different points in time.
- A method of transmitting motion information of dynamic nodes within the triangulation mesh to distant nodes using the triangulation mesh edges.

II. RELATED WORKS

Most existing triangulation mesh planning methods focus on fast re-planning. Kallmann [1] used A* in with a dynamically maintained Constraint Delaunay Triangulation [10] to update node position during runtime. Chen *et al.* [2] enhanced Dynamic Delaunay triangulation (DDT) [8] with a heuristic based algorithm for path planning to handle nodes that were newly identified by sensors. The Target Attraction Principle was proposed in [3] to position the nodes of a dual graph to a Constrained Delaunay Triangulation as a method to optimize the path cost.

Numerous anytime and incremental variants of A* search algorithms were reviewed in [4] path planning methods for a polygonal mesh. For instance, Anytime Repairing A* (ARA*) [15] attempts to return the best path found for a given time budget by iteratively improving an initial suboptimal solution. Incremental search algorithms such as D* Lite [13] reuses and repairs an initial solution found using A* at each re-planning cycle to adapt to the changes instead of re-planning from scratch. Field D* [14] was used in [5] for efficient re-planning within triangulation and tetrahedral mesh structures. Demyen *et al.* [6] introduced Triangulation Reduction A*, for path planning on a reduced dual graph of the environment's triangulation mesh. As an alternative to re-planning, [7] proposed the Gaps Filling algorithm to repair the previously found path by reconnecting broken path segments using Dijkstra's algorithm. It also employed an incremental insertion method [11] for efficient triangulation structure updates. To account for object dynamics, Timed A* was proposed in [16] for path planning in the dual graph of the Delaunay triangulation (DT). It considers the object dynamics by modifying the A*'s cost and heuristic function to include the ego vehicle's estimated time of arrival.

The above-mentioned methods do not allow for the consideration of non-adjacent nodes, and do not account for the changes to the triangulation mesh connectivity during planning. Distinct from previous work, our proposed method generates a sequence of connected channel segments to account for dynamic objects and their effect on the triangulation mesh connectivity.

III. METHODOLOGY

We assume a point representation of the static and dynamic nodes extracted from the environment, where each node represents a vertex, a point on the edge, or the centroid of the object. Each node is described by a 5D vector $\{x, y, \dot{x}, \dot{y}, r\}$, where r is the radius of the node. We also assume that all nodes follow a linear motion model. The commonly used

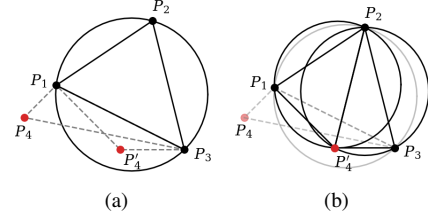


Fig. 1. Topological Event: a) topological event triggered by P_4 moving to P'_4 ; and b) violation repaired with edge flipping.

Delaunay Triangulation is employed to generate a triangulation mesh from these nodes. A Delaunay Triangulation structure over a set of points P must satisfy the condition that no $p \in P$ lies inside a triangle's circumcircle. The event which violates this condition is known as a topological event shown in Figure 1(a). This violation can be locally repaired by updating the edge connectivity as shown in Figure 1(b). Repairing the Delaunay Triangulation structure replaces the two triangles that cause the violation with two new triangles. This changes the edge connectivity of the triangles, thereby introducing new node adjacency and dual graph nodes.

Our objective is to find a sequence of spatially and temporally connected channel segments $\{C : C = \bigcup_{t=0}^N c'_t\}$, where $\{c'_t : c'_t = \bigcup_{j=0}^k \Delta_{t,j} | k \leq n\}$ is a subsequence of c_t , such that $\Delta_{t,j} \in c'_t$ is a subset of triangles $\Delta_{t,i} \in c_t$ that are unaffected by the changes in the edge connectivity of the triangulation mesh at time τ_t . The channel $\{c_t : c_t = \bigcup_{i=0}^n \Delta_{t,i}\}$, is a sequence of free triangles $\Delta_{t,i}$ in the triangulation mesh connectivity at τ_t , the triangle $\Delta_{t,0}$ contains the position of the ego vehicle and $\Delta_{t,n}$ contains the goal point. c_t is found by applying graph search on the dual graph of the triangulation mesh.

We consider $\Delta_{t,i}$ to be unaffected by changes in the triangulation mesh connectivity if i) there are no change to the edge connectivity of $\Delta_{t,i}$, $i \in \{0, \dots, n\}$ or ii) the first edge connectivity change of $\Delta_{t,i}$ occurred when the ego vehicle is located in $\Delta_{t,e} \in c_t$, and $e > i$. The first condition limits our consideration to the triangles that makes up the channel, since the changes to the triangles outside of the channel does not change the edge connectivity of the channel. The second condition excludes any $\Delta_{t,i}$ that had a change in edge connectivity after the ego vehicle already past it as these changes do not affect the ego vehicle.

Following the second condition, the last triangle of c'_t , *i.e.* $\Delta_{t,k}$, is determined by first finding the first triangle in c_t that had a change in its edge connectivity, $\Delta_{t,m}$, that satisfies the following: $\Delta_{t,m} = \Delta_{t,i} \in c_t | e \leq i$. If $e < m$, then $k = e$. If $e = m$ then $k = m - 1$, because we define c'_t to be triangles that are unaffected by changes in their edge connectivity. We do not consider $e > m$ as it is excluded by the second condition. $\Delta_{t,e}$ is the triangle that contains the position of the ego vehicle estimated at time τ_{t+1} , where τ_{t+1} is when the first edge connectivity change of $\Delta_{t,m}$ occurred.

Subsequent channel segment c'_{t+1} is similarly found by identifying the segment of c_{t+1} that is unaffected by changes in the edge connectivity of the triangulation mesh at time τ_{t+1} . Where c_{t+1} is from the expected triangulation mesh

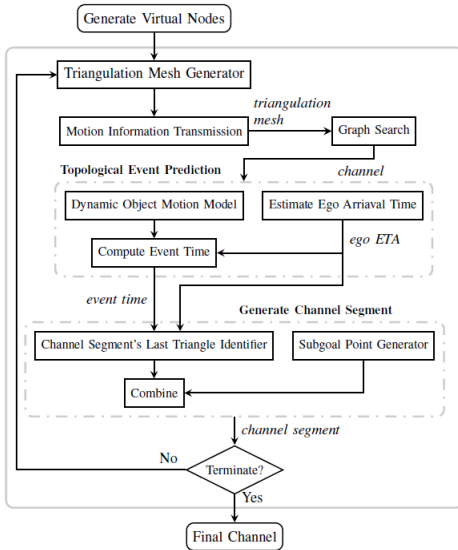


Fig. 2. Process diagram of the proposed method.

connectivity at τ_{t+1} under a linear motion model.

We ensure c'_t and c'_{t+1} is spatially and temporally connected by setting the last triangle of c'_t to be the first triangle of c'_{t+1} at τ_{t+1} , i.e. $\Delta_{t,k} = \Delta_{t+1,0}$.

The following sections describe the main modules of the system shown in Figure 2 in detail.

A. Generate Virtual Nodes

For autonomous driving applications, it's of interest to confine the ego vehicle to travel within a particular region instead of allowing it to travel within the entire free space. This module achieves this by identifying a boundary of the region that the vehicle will be allowed to drive in, which may be retrieved from objects in the free space; curbs, lane lines, barriers, and walls. The boundary is converted to a series of evenly spaced virtual static nodes, with the spacing to be narrow enough such that the ego vehicle cannot cross between the virtual nodes.

B. Triangulation Mesh Generator

We employed Delaunay Triangulation to generate a triangulation mesh from point representation of the static and dynamic objects extracted from the environment and constructs the corresponding dual graph. The dual graph has a node corresponding to each triangle of the mesh and an edge for each edge in the mesh that separates a pair of triangles. Target Attraction Principle [3] is used to position the dual graph nodes since the cost of reaching the triangles during graph search is computed based on the position of the dual graph node. Constrained Delaunay Triangulation or Dynamic Delaunay Triangulation can also be used as alternatives to construct the triangulation mesh.

C. Motion Information Transmission

We achieve this by projecting the velocity \mathbf{v}_i of each node n_i onto the positional vectors $\mathbf{p}_{i,j}$ to their adjacent nodes n_j , where $\mathbf{p}_{i,j}$ is the positional vector from n_i to n_j . We denote the projected velocity vector as \mathbf{v}'_i . To preserve the heading

information of n_i , \mathbf{v}'_i will assume the direction of \mathbf{v}_i , thus $\mathbf{v}'_i = \|\mathbf{v}_i\| \cos \theta \hat{\mathbf{v}}_i = \cos \theta \mathbf{v}_i$. The effect of the proximity of n_i to n_j is accounted for by multiplying \mathbf{v}'_i by $\frac{\alpha}{\|\mathbf{p}\|+\alpha}$, $\alpha \geq 0$, so that $\|\mathbf{v}'_i\|$ decreases as n_i is further away from n_j . The α is to balance the effect of velocity and proximity. Furthermore, the heading of node n_i relative to n_j is accounted for by \mathbf{v}'_i by a term $|\frac{\pi}{2} - \theta|^\beta$, where $\theta \in [-\frac{\pi}{2}, \frac{\pi}{2}]$, $\beta \geq 0$, and θ is the angle between \mathbf{v}_i and $\mathbf{p}_{i,j}$. If $\theta \notin [-\frac{\pi}{2}, \frac{\pi}{2}]$, then we multiply \mathbf{v}'_i by 0 since n_i is moving away from n_j . The β is used to tune this term such that the effect of \mathbf{v}_i diminishes as it becomes more orthogonal to $\mathbf{p}_{i,j}$,

$$\mathbf{v}'_i = \begin{cases} \frac{\alpha}{\|\mathbf{p}\|+\alpha} |\frac{\pi}{2} - \theta|^\beta \cos \theta \mathbf{v}_i & \text{if } \theta \in [-\frac{\pi}{2}, \frac{\pi}{2}] \\ 0 & \text{otherwise} \end{cases}. \quad (1)$$

To transmit the motion of the n_i to n_j , we set the velocity vector \mathbf{v}_j of n_j to \mathbf{v}'_i if $\|\mathbf{v}_j\| < \|\mathbf{v}'_i\|$ and that $\mathbf{v}_i \cdot \mathbf{p}_{i,j} > 0$, as expressed below,

$$\mathbf{v}_j = \begin{cases} \mathbf{v}'_i & \text{if } \|\mathbf{v}_j\| < \|\mathbf{v}'_i\| \\ \mathbf{v}_j & \text{otherwise} \end{cases}. \quad (2)$$

Figure 3 shows an example of applying this equation onto a set of nodes, where the velocity information of the dynamic nodes, red, green, and blue is projected onto the nodes around them.

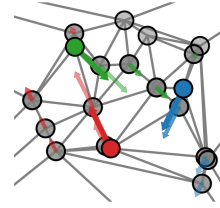


Fig. 3. Motion information transmission example. Colored nodes are dynamic nodes, grey nodes are static nodes. All nodes with the same colored arrow received velocity information from the same node.

D. Graph Search

This module finds an initial c_t that leads from start to goal within the triangulation mesh connectivity at τ_t by searching through the dual graph of triangulation mesh. We used Timed A* [16], which accounts for the path cost change due to object dynamics by computing $f(t_{eta}) = g(t_{eta}) + h(t_{eta})$, where t_{eta} is the estimated time of arrival of the ego vehicle to a triangle. Additionally, it ensures that the distance between two nodes is wide enough to allow the ego vehicle to cross by checking t_{eta} against the time interval in which the length of the corresponding Delaunay Triangulation edge is above a threshold.

E. Topological Event Prediction

This module determines τ_{t+1} , the time of the first edge connectivity change of $\Delta_{t,m}$. Note that the triangle $\Delta_{t,e}$ contains the ego vehicle position, and we have limited our consideration to $e \leq m$. Therefore, we can efficiently find τ_{t+1} and $\Delta_{t,m}$ by iterating through $\Delta_{t,i} \in c_t$ to check if there is a change in edge connectivity before the time that the ego vehicle arrives at $\Delta_{t,i}$. If there is a change, $\Delta_{t,m} = \Delta_{t,i}$, otherwise $i = i + 1$. We present this process in Algorithm 1.

1) *In-circle Test*: The in-circle test [17] defined in (3) is a standard test used to check if a 4th point lies within the circumcircle of a triangle. This corresponds to the `incircleTest()` function in Algorithm 1.

The in-circle test is performed by calculating the determinant of a 4×4 matrix, constructed from the position of the 4 nodes. Where (x_i, y_i) , $i \in \{1, 2, 3\}$ are the position of the triangle vertices. (x_4, y_4) is the position of the 4th point. The determinant of the 2nd matrix corrects the signs of the in-circle test such that it is insensitive to the ordering of the first three points. If $\gamma = 0$, the 4th point is co-circular with the circumcircle, where $\gamma < 0$ and $\gamma > 0$, respectively, indicate that the 4th point is inside or outside the circumcircle.

$$\gamma = \det \begin{bmatrix} 1 & x_1 & y_1 & x_1^2 + y_1^2 \\ 1 & x_2 & y_2 & x_2^2 + y_2^2 \\ 1 & x_3 & y_3 & x_3^2 + y_3^2 \\ 1 & x_4 & y_4 & x_4^2 + y_4^2 \end{bmatrix} \times \det \begin{bmatrix} 1 & x_1 & y_1 \\ 1 & x_2 & y_2 \\ 1 & x_3 & y_3 \end{bmatrix} \quad (3)$$

2) *Compute Event Time*: Algorithm 1 computes τ_{t+1} by performing the in-circle test on each $\Delta_{t,i} \in c_t$ using $(x_i(t), y_i(t))$, $i \in \{1, \dots, 4\}$, where $t \in [\tau_t, t_{eta}]$. $(x_i(t), y_i(t))$ is the expected position of the vertices of $\Delta_{t,i}$ and the point tested by the in-circle test at time t . Time t is a time point sampled at even intervals from τ_t to t_{eta} . The t_{eta} is the ego vehicle's estimated time of arrival at $\Delta_{t,i}$ because we only consider the topological event that occurred before the ego vehicle arrives at $\Delta_{t,i}$.

Algorithm 1: Compute Topological Event Time

```

Input:  $c_t$ , sample resolution
Output:  $\tau_{t+1}, \Delta_{t,m}$ 
def vertices( $\Delta_{t,i}$ ):
   $\square$  return vertices of  $\Delta_{t,i}$ 
def getETA( $\Delta_{t,i}$ ):
   $\square$  return  $t_{eta}$ 
def getNeighbors( $\Delta_{t,i}$ ):
   $\square$  return All vertices of the adjacent triangles that are not also
  vertices of  $\Delta_{t,i}$ 
def dynamicModel( $p1, p2, p3, p4, t$ ):
   $\square$  return position of input points at time  $t$ 
def incircleTest( $a, b, c, p$ ):
   $\square$  return  $\gamma < 0$ 
def main( $c_t, sample\ resolution$ ):
  for  $\Delta_{t,i}$  in  $c_t$  do
     $a, b, c =$  vertices( $\Delta_{t,i}$ )
     $t_{eta} =$  getETA( $\Delta_{t,i}$ )
    for  $p$  in getNeighbors( $\Delta_{t,i}$ ) do
      for  $\tau$  in range( $0, t_{eta}, sample\ resolution$ ) do
         $a, b, c, p =$  dynamicModel( $a, b, c, p, \tau$ )
        if incircleTest( $a, b, c, p$ ) then
           $\square$  return  $\tau, \Delta_{t,i}$ 
  return None

```

Algorithm 1 terminates if the in-circle test finds a topological event, in which τ_{t+1} is the returned time and $\Delta_{t,m}$ is the returned triangle. Algorithm 1 also terminates if no event is found for any triangle within the channel, which indicates that c_t is the final segment of C .

3) *Dynamic Object Motion Model*: This module corresponds to the `dynamicModel()` function in Algorithm 1.

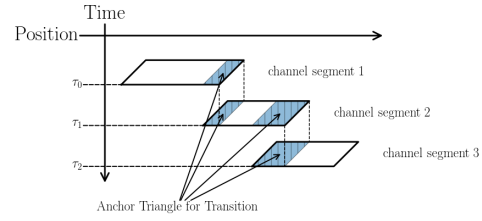


Fig. 4. Conceptual diagram of the overall generated channel C . The anchor triangles mark the overlapping triangles in each transition.

This returns $(x_i(t_j), y_i(t_j))$, which is a function that estimates the position of nodes at time t_j , $t_j \in [\tau, t_{eta}]$, $\mathbf{p}^i(\mathbf{t}) = \mathbf{p}_0^i + f(v, t)$, where $f(v, t)$ is a linear or nonlinear function. v is the current velocity of the object, and t is time. In our implementation, we used a linear model, *i.e.* $f(v, t) = \mathbf{v}^i t$, to estimate the position of the nodes.

4) *Estimate Ego Arrival Time*: This module corresponds to the `getETA()` function in Algorithm 1. It estimates the time of arrival of the ego vehicle t_{eta} to $\Delta_{t,i}$ following the linear motion model. The Target Attraction Principle proposed by [3] is used to position the dual graph node that represents each triangle. t_{eta} is estimated by taking the ego vehicle's speed over the travel distance from the starting position to the dual graph node that corresponds to $\Delta_{t,i}$.

F. Generate Channel Segment

Module III-F.1 identifies c'_t by finding triangle $\Delta_{t,k} \in c_t$, which is the last triangle of c'_t . Additionally, since path planners typically requires a point to navigate to, module III-F.2 identifies a subgoal point within $\Delta_{t,k}$ for path planning.

1) *Channel Segment's Last Triangle Identifier*: $\Delta_{t,k}$ is found with the following:

- if $e < m$, then $\Delta_{t,k} = \Delta_{t,e}$, where m is the index of $\Delta_{t,m} \in c_t$;
- if $e \geq m$, then $\Delta_{t,k} = \Delta_{t,m-1}$.

To spatially and temporally connect c'_t to c'_{t+1} , we consider the last triangle of c'_t to also be the first triangle of c'_{t+1} , $\Delta_{t,k} = \Delta_{t+1,0}$. Therefore, $\Delta_{t,k}$ serves as the triangle that transitions from c'_t to c'_{t+1} at time τ_{t+1} .

2) *Sub-Goal Point Generation*: Since local planner typically requires a point to navigate to, this module chooses a collision-free point inside the $\Delta_{t,k}$, that is closest to the estimated ego vehicle position at τ .

G. Terminal Condition

Algorithm 1 will return None when the input c_t leads to the goal point without any of the triangles in c_t seeing a topological event. This means that $C = \{c'_0, \dots, c'_t\}$, where each channel $c \in C$ can be used to plan a path segment.

Otherwise, our system finds c'_{t+1} by repeating from module III-B using the expected position of the starting node and the dynamic objects at τ_{t+1} found by module III-E. Our system as shown in Figure 2 may also choose to terminate early to limit the planning horizon when the first n channel segments c' is found, or when the predicted $\tau_{t+1} > \tau_{threshold}$.

Figure 4 demonstrates a conceptual understanding of C . Each c'_t is valid for from time τ_t until the next time of topological event τ_{t+1} . To transition from one channel to

the next, the last triangle $\Delta_{t,k}$ of c'_t will overlap with the first triangle of the next channel segment c'_{t+1} .

IV. EXPERIMENTS

We carried out two experiments to verify the effectiveness of our proposed method against a synthetic set of scenarios and a set of real world scenarios from the nuScenes dataset [18]. We compare the channels generated by our proposed method against the channels generated by existing triangulation-based planning methods that uses A* and Timed A* to search for the channels. Because there are no metrics to directly evaluate channels, the channels are evaluated based on the performance of the path planned using those channels. The Funnel Algorithm [19] is used to produce the path using the channel generated by each method. We add an offset to the vertices of the funnel as padding for collision avoidance. Note that the simplicity of the funnel algorithm cannot guarantee the path to be collision free. The channels are compared in terms of rate of task completion, the time taken to complete each task, rate of successfully planning a path, and rate of collision. All experiments are implemented using Python and carried out on a computer with a 3.6GHz CPU and 32GB of memory.

A. Scenarios

1) *Synthetic*: This experiment is a set of 200 synthetic scenarios to test the long-term planning capability of our proposed method by introducing frequent changes in the triangulation mesh connectivity. These scenarios have between 10 to 20 pedestrians with randomized position and speed, ranging from 0.25 m/s to 1 m/s crossing perpendicularly to a 30 m straight road. The ego vehicle is tasked to navigate to the end of the road at 2 m/s within a simulation time limit of 25 s.

2) *nuScenes*: This experiment is a set of 150 real-world scenarios from the nuScenes dataset [18] to test the proposed method's performance in realistic scenarios. These scenarios are collected from typical driving conditions such as highway, intersections, and parking lots. Each scenario is 20 s long, annotated at 2 Hz. We linearly interpolated the position of objects in the scenario at 10 Hz for higher temporal resolution. All dynamic objects' motion after the annotated 20 s is assumed to be linear. The ego vehicle is tasked to navigate, starting from the data collection vehicle's pose at $t = 0$ to the pose at $t = 20$ at the average velocity of the data collection vehicle within 30 s in simulation time. The experiment environment is a rectangular region that encloses the start and goal point. We confine the ego vehicle's motion to the road by placing virtual static nodes on the boundary of the drivable area map layer of the nuScenes dataset. On average, each scenario contains 389 nodes, where 55 of which are dynamic or static objects identified from the environment.

B. Result

This section presents the comparison results obtained based on the Synthetic and nuScenes scenarios. A* is expected to result in a higher completion rate, higher success

rate, and lower task time as it ignores the dynamic objects. Because A* ignores dynamic objects, it is also expected to result in a higher collision rate. As such, a desirable method, ideally, should have comparable completion rate, success rate, and task time to those of A*, while resulting in a lower collision rate. Figure 5 summarizes the comparison results between A*, Timed A* [16], and our method against a Synthetic dataset and a real-world dataset from nuScenes.

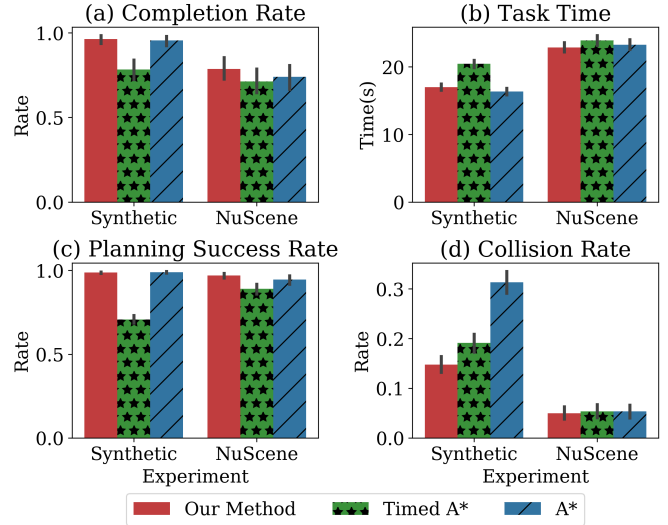


Fig. 5. Experimental results in comparison to Timed A* [16] and A* against a Synthetic dataset and a real-world dataset from nuScenes.

1) *Synthetic*: Our method completed 96.3% of tasks at an average time of 17 s, Timed A* completed 78.6% of the tasks at an average time of 21 s, and A* completed 95.5% of the task at 16.3 s. Our method produced spatial constraints that allowed the local planner to find a valid plan in 98.7% of the planning cycles, whereas Timed A* was 70.7% and A* at 98.9%.

The Timed A* based method has a lower success rate of finding a path at each planning cycle. This is because Timed A* looks for a channel based on the future state of the triangulation mesh, while it provides the path planner with a channel at the present state. The channel width at the present state may not be large enough to allow the ego vehicle to pass, thus the path planner fails. The path planner failure cases for both our method and A* based method are situations where the ego vehicle needed to stop and wait for dynamic objects in front of it to pass before it can proceed.

Since A* ignores the motion of dynamic objects when it generates the spatial constraint, it may result in unfavorable paths that are not suitable for autonomous driving. The effect of this is evident in its high collision rate of 31.3%, whereas our method is at 14.8% and Timed A* at 19.1%. Figure 6 shows an example of the unfavorable situation, where the A* method shown by the blue dashed line resulted in a path that ignored the motion of the dynamic object until $t = 3.6$. It was then forced to make a sudden course change at $t = 4.0$ because the previous path was no longer feasible. The path generated by our method shown in the red solid

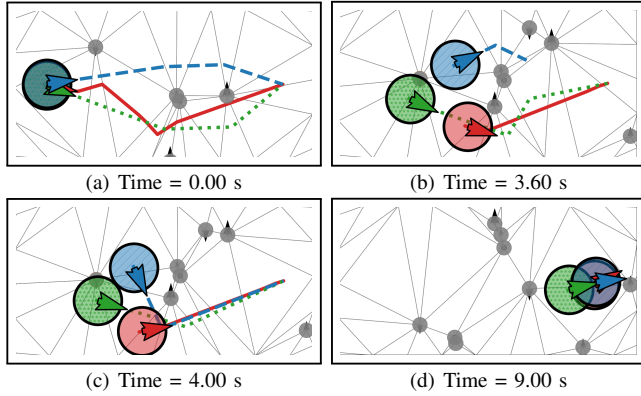


Fig. 6. Straight Scenario Example. Our method (red solid), Timed A* (green dotted), A* (blue dashed). Grey circles (pedestrians).

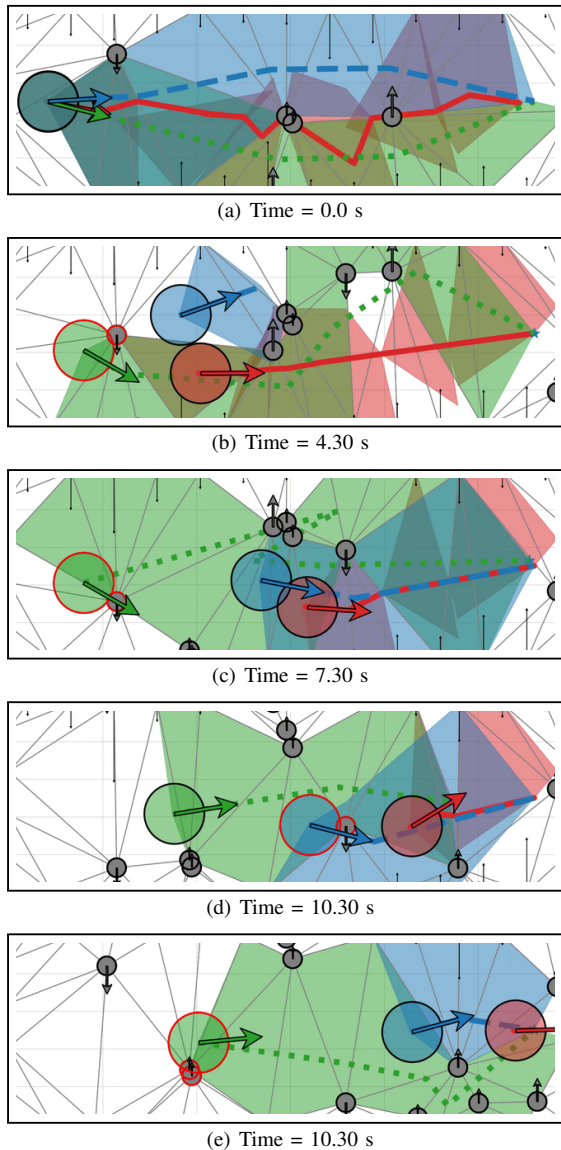


Fig. 7. A sample scenario, in which both A* and Timed A* fail. Our method (red solid), Timed A* (green dotted), A* (blue dashed). Grey circles (pedestrians). The colliding objects are marked by red circumference.

line and Timed A* shown in the green dotted line both moved in another direction to account for the pedestrian motion and have anticipated that the path will not be feasible at a later time. Figure 7 also shows a similar scenario, in which both Timed A* and A* collide with the crossing objects due to invalid triangulations and lack of collision checks for dynamic objects, respectively. Note that some of the collisions are contributed by the simplicity of the path planner not providing sufficient spacing when passing an object. A more sophisticated local planner would result in fewer or no collisions.

2) *nuScenes*: Our method completed the task 78.7%, outperforming Timed A*, which was at 71.3% and A* at 74.1%. The average time of completion is similar for all three methods; 22.9 s for our method, 23.9 s for Timed A*, and 23.25 s for A*. Using the channel produced by our method, the local planner was able to find a path 97% of the time, where it was 89.1% for Timed A* and 94.5% for A*. Because most scenarios are similar to a lane following task, the collision rate is similar for all three methods; 5% for our method, and 5.3% for both Timed A* and A*. This is expected as pedestrians or other objects mostly move along the road in these scenarios, which is an easier motion planning task compared to pedestrian crossing or lane-changing scenarios. This is also shown in Figure 8, in which the objects do not cross the lane for a greater portion of the scenario.

Figure 9 shows an example of the *nuScenes* scenario where Timed A* identified a feasible channel, however, the channel was based on the current triangulation mesh connectivity. This channel did not have sufficient space to allow the local planner to find a path, thus the local planner was unable to find a path until $t = 5.3$. At $t = 13.4$, a pedestrian was about to cross the road, our proposed method accounted for this when generating a channel and tried to maneuver around the pedestrian, as shown in the slight turn in its path. In contrast, A* would've only stopped when the spacing to cross becomes too narrow.

V. CONCLUSIONS

In this paper, we presented a novel method to generate spatial constraints for motion planning in dynamic environments. This method can enhance other planning modules. For example, it can act as a preprocessor to generate spatial constraints as inputs or to prune candidate trajectories generated by the motion planner. It can perform mission planning to find a global route or to use it as a safeguard against semantic map failures that may be caused by dynamic changes in the map (e.g. road obstruction and construction zones). Furthermore, the proposed system's modularity allows for adding, removing, and replacing the various modules as desired. We evaluated our method in a set of real-world scenarios simulated based on an autonomous driving dataset. The result shows that using our method can obtain a more stable, long-term plan that yields a higher task completion rate, faster travel time, higher planning success rate, and fewer collisions compared to other existing methods.

REFERENCES

- [1] M. Kallmann, "Path planning in triangulations," in *Proceedings of the IJCAI workshop on reasoning, representation, and learning in computer games*, 2005, pp. 49–54.
- [2] J. Chen, C. Luo, M. Krishnan, M. Paulik, and Y. Tang, "An enhanced dynamic delaunay triangulation-based path planning algorithm for autonomous mobile robot navigation," in *Intelligent Robots and Computer Vision XXVII: Algorithms and Techniques*, vol. 7539. International Society for Optics and Photonics, 2010, p. 75390P.
- [3] H. Yan, H. Wang, Y. Chen, and G. Dai, "Path planning based on constrained delaunay triangulation," in *2008 7th World Congress on Intelligent Control and Automation*. IEEE, 2008, pp. 5168–5173.
- [4] M. Kallmann and M. Kapadia, "Navigation meshes and real-time dynamic planning for virtual worlds," in *ACM SIGGRAPH 2014 Courses*, 2014, pp. 1–81.
- [5] S. Perkins, P. Marais, J. Gain, and M. Berman, "Field D* path-finding on weighted triangulated and tetrahedral meshes," *Autonomous agents and multi-agent systems*, vol. 26, no. 3, pp. 354–388, 2013.
- [6] D. Demyen and M. Buro, "Efficient triangulation-based pathfinding," in *Aaai*, vol. 6, 2006, pp. 942–947.
- [7] P. Broz, M. Zemek, I. Kolingerová, and J. Szkandera, "Dynamic path planning with regular triangulations," *Machine Graphics & Vision*, vol. 24, no. 3/4, pp. 119–142, 2014.
- [8] O. Devillers, S. Meiser, and M. Teillaud, "Fully dynamic delaunay triangulation in logarithmic expected time per operation," *Computational Geometry*, vol. 2, no. 2, pp. 55–80, 1992.
- [9] M. A. Mostafavi, C. Gold, and M. Dakowicz, "Delete and insert operations in Voronoi/Delaunay methods and applications," *Computers & Geosciences*, vol. 29, no. 4, pp. 523–530, 2003.
- [10] L. P. Chew, "Constrained Delaunay triangulations," *Algorithmica*, vol. 4, no. 1-4, pp. 97–108, 1989.
- [11] H. Edelsbrunner and N. R. Shah, "Incremental topological flipping works for regular triangulations," *Algorithmica*, vol. 15, no. 3, pp. 223–241, 1996.
- [12] M. Likhachev, D. I. Ferguson, G. J. Gordon, A. Stentz, and S. Thrun, "Anytime Dynamic A*: An anytime, replanning algorithm," in *ICAPS*, vol. 5, 2005, pp. 262–271.
- [13] S. Koenig and M. Likhachev, "D* Lite," *Aaai/iaai*, vol. 15, 2002.
- [14] D. Ferguson and A. Stentz, "The Field D* algorithm for improved path planning and replanning in uniform and non-uniform cost environments," *Robotics Institute, Carnegie Mellon University, Pittsburgh, PA, Tech. Rep. CMU-RI-TR-05-19*, 2005.
- [15] M. Likhachev, G. J. Gordon, and S. Thrun, "ARA*: Anytime A* with provable bounds on sub-optimality," in *Advances in neural information processing systems*, 2004, pp. 767–774.
- [16] C. Cao, P. Trautman, and S. Iba, "Dynamic channel: A planning framework for crowd navigation," in *2019 International Conference on Robotics and Automation (ICRA)*. IEEE, 2019, pp. 5551–5557.
- [17] L. Guibas and J. Stolfi, "Primitives for the manipulation of general subdivisions and the computation of Voronoi," *ACM transactions on graphics (TOG)*, vol. 4, no. 2, pp. 74–123, 1985.
- [18] H. Caesar, V. Bankiti, A. H. Lang, S. Vora, V. E. Liong, Q. Xu, A. Krishnan, Y. Pan, G. Baldan, and O. Beijbom, "nuScenes: A multimodal dataset for autonomous driving," *arXiv preprint arXiv:1903.11027*, 2019.
- [19] J. Hershberger and J. Snoeyink, "Computing minimum length paths of a given homotopy class," *Computational geometry*, vol. 4, no. 2, pp. 63–97, 1994.

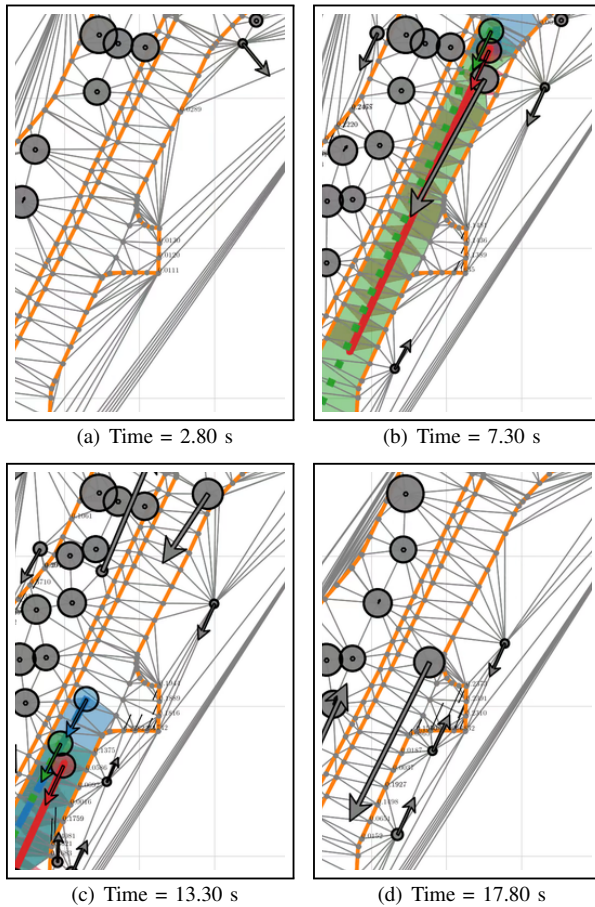


Fig. 8. A Sample nuScenes Lane Following Scenario. Our method (red solid), Timed A* (green dotted), A* (blue dashed). Grey circles (dynamic or static objects).

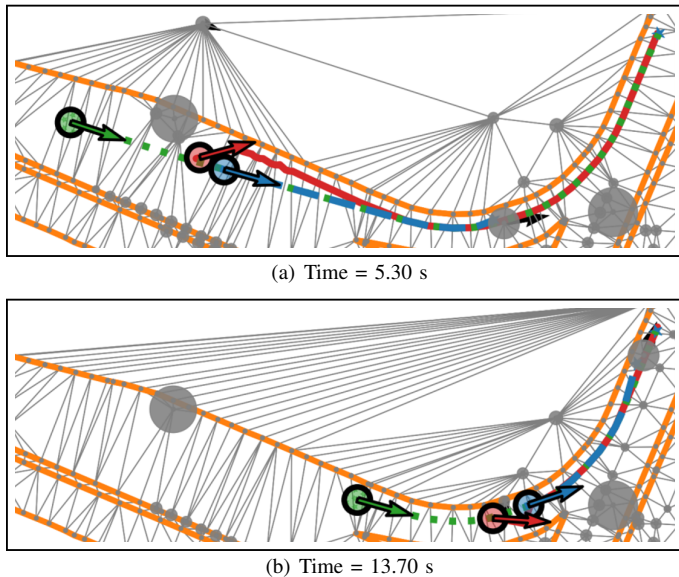


Fig. 9. nuScenes Scenario Example. Our method (red solid), Timed A* (green dotted), A* (blue dashed). Grey circles (dynamic or static objects).